J|A|C|S
ARTICLES
Published on Web 12/14/2005

Excited-State Potential Energy Surface for the Photophysics of Adenine

Lluís Blancafort

Contribution from the Institut de Química Computacional, Departament de Química, Universitat de Girona, ES-17071 Girona, Spain

Received July 25, 2005; E-mail: lluis.blancafort@udg.es

Abstract: The decay paths on the singlet excited-state surface of 9H-adenine and the associated energy barriers have been calculated at the CAS−PT2//CASSCF level. There are three fundamental paths for the photophysics: two paths for the ^1L_b state which are virtually barrierless at the present level of theory and correspond to formation of the (n,π^*) intermediate and direct decay to the ground state and a third path for ground-state decay of the (n,π^*) state with an activation barrier of approximately 0.1 eV. The ^1L_a state, which has the largest oscillator strength, either decays directly to the ground state or contributes indirectly to the excited-state lifetime by populating the two other states. The results are used to interpret the photophysics in terms of an excited-state plateau for the ^1L_b state that corresponds to the short-lived excited-state component (approximately 0.1 ps) and a well (i.e., a proper minimum) for the (n,π^*) state that gives rise to the long component (1 ps or more). The direct decay to the ground state of the ^1L_b state is probably the decay channel invoked to explain the experimental wavelength dependence of the relative amplitudes of the two components. In addition to that, the excited-state component in the nanosecond range detected in the time-resolved photoelectron spectrum is proposed to be a triplet (π,π^*) state formed after intersystem crossing from the singlet (n,π^*) state.

Introduction

The development of spectroscopic methods with femtosecond resolution has directed great attention toward the spectroscopy of the DNA bases due to the interest in understanding the photophysics of these important building blocks of life.[1] Their general characteristic is the short lifetimes of the singlet excited species, which lie in the picosecond and sub-picosecond range.[2,3] In addition to that, the spectroscopic details of the different bases are rather complex. In the case of the 9H isomer of adenine (briefly: adenine), the gas-phase spectroscopy was first described with a monoexponential decay,[3,4] whereas later results agree on a biexponential decay of the signals in the picosecond regime.[5−9] A dependence of the decay on the excitation wavelength has been also observed.[5,6,8] The challenge for theory, especially for potential-energy surface (PES) calculations, is to explain this behavior. For adenine, several recent papers[10−12] have provided such an explanation by locating, at different levels of theory, the crossings between the ground and excited states (conical intersections) where radiationless decay can take place. In particular, two different conical intersections have been located in recent CAS-PT2//CASSCF studies[10,12] (combination of CASSCF, complete active space self-consistent field, optimizations and CAS-PT2, second-order perturbation of the CASSCF reference, energies). To explain the short lifetimes, low barriers were estimated between the excited-state minima, which are the main species detected experimentally, and the intersections. Similar conclusions were provided by a different study[11] that combined TD-DFT (time-dependent density functional theory) with DFT/MRCI (DFT/multireference configuration interaction). However the purpose of the present paper is to show that the currently available computational methodology allows for a more detailed characterization of the PES. In mechanistic terms, by improving the accuracy of the calculation it is possible to estimate which are the most relevant paths in the experiments. More importantly, the calculations can help to improve the models used to interpret the time and vibronically resolved spectroscopy.

Adenine has three low-lying singlet excited states, two of (π,π^*) type (a ^1L_b and a ^1L_a state) and an (n,π^*) one. The most recent time-resolved spectra in the gas phase have been fitted to a doubly exponential decay, with a short component with a lifetime up to 100 fs assigned to a (π,π^*) state and a longer component between 750 fs and more than 2 ps assigned to the

(1) Crespo-Hernández, C. E.; Cohen, B.; Hare, P. M.; Kohler, B. *Chem. Rev.* **2004**, *104*, 1977−1202.
(2) Pecourt, J. M. L.; Peon, J.; Kohler, B. *J. Am. Chem. Soc.* **2001**, *123*, 10370−10378.
(3) Kang, H.; Lee, K. T.; Jung, B.; Ko, Y. J.; Kim, S. K. *J. Am. Chem. Soc.* **2002**, *124*, 12958−12959.
(4) Kang, H.; Jung, B.; Kim, S. K. *J. Chem. Phys.* **2003**, *118*, 6717−6719.
(5) Ullrich, S.; Schultz, T.; Zgierski, M. Z.; Stolow, A. *Phys. Chem. Chem. Phys.* **2004**, *6*, 2796−2801.
(6) Ullrich, S.; Schultz, T.; Zgierski, M. Z.; Stolow, A. *J. Am. Chem. Soc.* **2004**, *126*, 2262−2263.
(7) Canuel, C.; Mons, M.; Piuzzi, F.; Tardivel, B.; Dimicoli, I.; Elhanine, M. *J. Chem. Phys.* **2005**, *122*, 074316.
(8) Samoylova, E.; Lippert, H.; Ullrich, S.; Hertel, I. V.; Radloff, W.; Schultz, T. *J. Am. Chem. Soc.* **2005**, *127*, 1782−1786.
(9) Ritze, H.-H.; Lippert, H.; Samoylova, E.; Smith, V. R.; Hertel, I. V.; Radloff, W.; Schultz, T. *J. Chem. Phys.* **2005**, *122*, 224320.
(10) Perun, S.; Sobolewski, A. L.; Domcke, W. *J. Am. Chem. Soc.* **2005**, *127*, 6257−6265.
(11) Marian, C. M. *J. Chem. Phys.* **2005**, *122*, 104314.
(12) Chen, H.; Li, S. *J. Phys. Chem. A* **2005**, *109*, 8443−8446.

10.1021/ja054998f CCC: $33.50

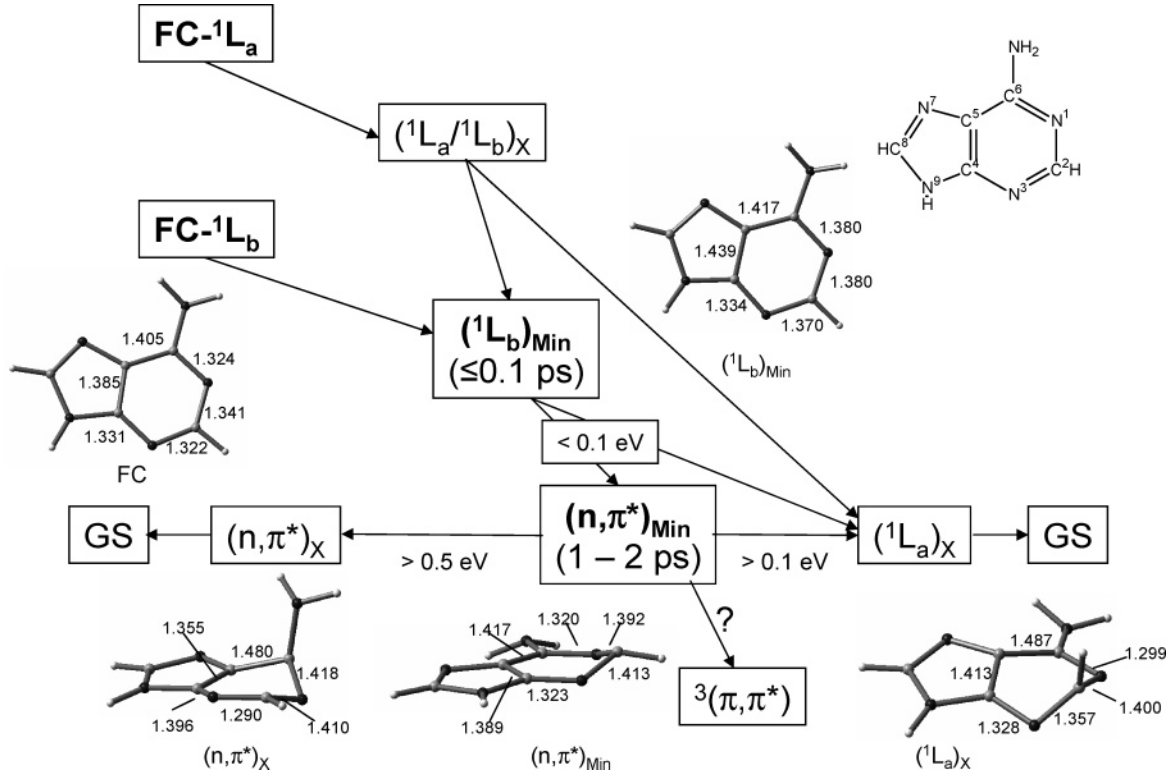

Figure 1. Overview of the reaction paths on the excited-state PES for the deactivation of the ^1L_a and ^1L_b states of adenine, including the proposed assignment of the two minima to the experimental lifetimes.

(n,π^*) state.[5−9] The relative amplitudes of the components and the lifetime of the long component depend on the excitation wavelength.[5,6] Thus, the amplitude of the short component decreases significantly when the excitation wavelength changes from 267 to 250 nm, and the lifetime of the long component decreases from approximately 2 ps to 0.75−1.0 ps between 272- and 267-nm excitation.[8] In addition to that, the main feature of the vibronically resolved spectrum is the presence of a few low-lying bands that show almost no vibrational progression,[13−18] and the measured lifetime of one of these bands (assigned to the (π,π^*) state) is 9 ps.[15] Numerous spectroscopic studies have also been carried out in water, where in general a monoexponential decay is assigned to the 9H tautomer of adenine.[19−21] However the present computational study focuses on the gas-phase photophysics of adenine, and the results in solvent will not be considered here in detail.

On the theoretical side, the first PES studies located different minima for the ^1L_b and (n,π^*) excited states.[22,23] The conical intersections located in more recent studies[10−12] are characterized by out of plane bends of the C_2 and N_1 atoms and correlate with the ^1L_a and (n,π^*) states, respectively. The overall picture is that the S_1 PES of adenine is very flat, and the minima of the (^1L_b) and (n,π^*) states are separated from the intersections by low barriers estimated to be of the order of 0.1 eV. The (n,π^*) minimum is more stable than the (^1L_b) one by approximately 0.2 eV, which justifies the assignment of the long and short-lived components, respectively. The fast conversion from the (^1L_b) to the (n,π^*) state is justified by the presence of a conical intersection between the two states, which are strongly vibronically mixed, and an extremely short lifetime for the ^1L_a state is proposed.[10] Higher-energy paths involving bond-breaking processes in the rings have been also studied at the CASSCF//CAS-PT2 level.[24]

The present study uses the CAS-PT2//CASSCF methodology. Thus the structures are optimized at the CASSCF level, and dynamic correlation is introduced with single point CAS−PT2 calculations for a better estimation of the energy. In contrast to previous studies, the minimum energy paths (MEP) are calculated at the CASSCF level, and the resulting CAS-PT2//CASSCF profiles can be used to connect the critical points unambiguously and estimate the energy barriers that separate them. The resulting picture is given in Figure 1, which shows the connectivity (not the surface topography) of the different minima and intersections and the estimated CAS-PT2//CASSCF barriers. The results suggest that the reason behind the short lifetime of the ^1L_b minimum, labeled $\mathbf{(^1L_b)_{Min}}$, is not only its higher energy relative to the minimum of the (n,π^*) state, $\mathbf{(n,\pi^*)_{Min}}$ but also the presence of a virtually barrierless channel

(13) Kim, N. J.; Jeong, G.; Kim, Y. S.; Sung, J.; Kim, S. K.; Park, Y. D. *J. Chem. Phys.* **2000**, *113*, 10051−10055.
(14) Plützer, C.; Nir, E.; de Vries, M. S.; Kleinermanns, K. *Phys. Chem. Chem. Phys.* **2001**, *3*, 5466−5469.
(15) Lührs, D. C.; Viallon, J.; Fischer, I. *Phys. Chem. Chem. Phys.* **2001**, *3*, 1827−1831.
(16) Nir, E.; Plützer, C.; Kleinermanns, K.; de Vries, M. *Eur. Phys. J. D* **2002**, *20*, 317−329.
(17) Plützer, C.; Kleinermanns, K. *Phys. Chem. Chem. Phys.* **2002**, *4*, 4877−4882.
(18) Kim, N. J.; Kang, H.; Park, Y. D.; Kim, S. K. *Phys. Chem. Chem. Phys.* **2004**, *6*, 2802−2805.
(19) Gustavsson, T.; Sharonov, A.; Onidas, D.; Markovitsi, D. *Chem. Phys. Lett.* **2002**, *356*, 49−54.
(20) Cohen, B.; Hare, P. M.; Kohler, B. *J. Am. Chem. Soc.* **2003**, *125*, 13594−13601.
(21) Pancur, T.; Schwalb, N. K.; Renth, F.; Temps, F. *Chem. Phys.* **2005**, *313*, 199−212.
(22) Broo, A. *J. Phys. Chem. A* **1998**, *102*, 526−531.
(23) Mennucci, B.; Toniolo, A.; Tomasi, J. *J. Phys. Chem. A* **2001**, *105*, 4749−4757.
(24) Perun, S.; Sobolewski, A. L.; Domcke, W. *Chem. Phys.* **2005**, *313*, 107−112.

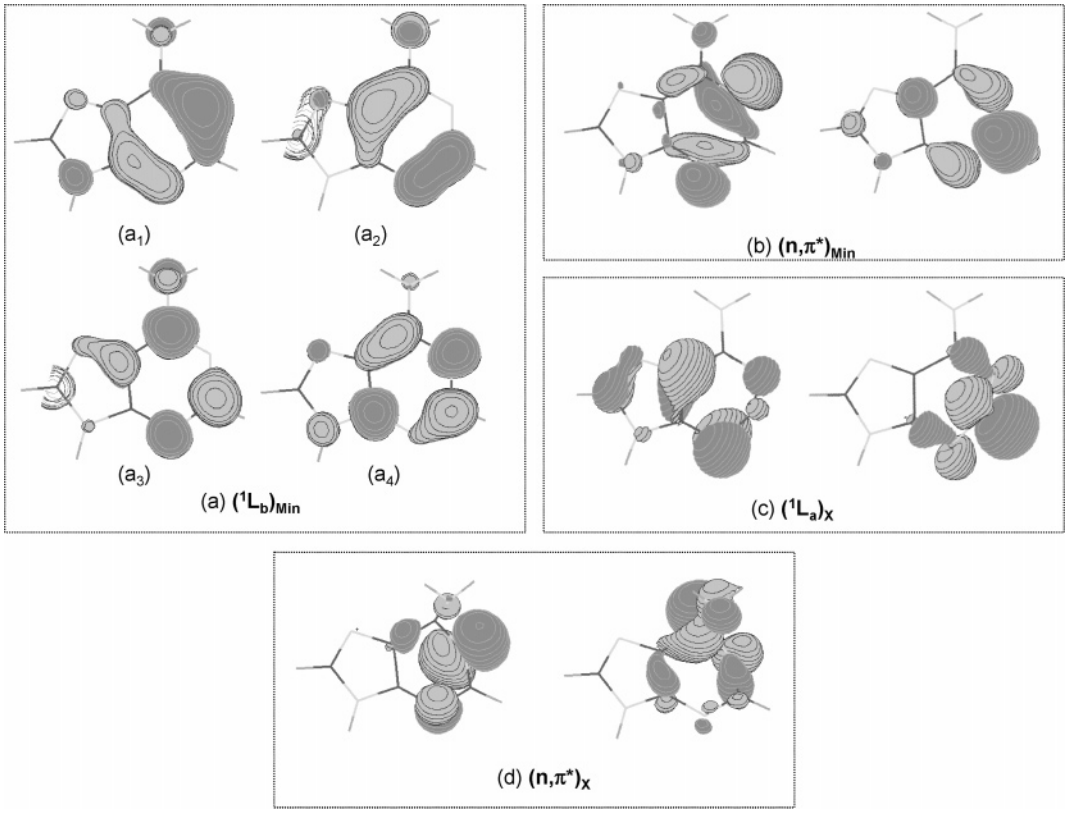

Figure 2. Orbitals involved in the excitations at the optimized structures. Dominant configurations for a: $a_1 \rightarrow a_3$; $a_1 \rightarrow -a_4$.

to the intersection of ^1L_a type, $\mathbf{(^1L_a)_X}$. Remarkably, this path has not been explicitly considered in any of the previous computational studies. Moreover, the path from $\mathbf{(^1L_b)_{Min}}$ to $\mathbf{(n,\pi^*)_{Min}}$ also has a very small or no barrier. The competition between the two different decay channels for $\mathbf{(^1L_b)_{Min}}$ may therefore explain the observed dependence of the relative amplitudes of the components on the excitation wavelength.

In contrast to the decay paths characterized for $\mathbf{(^1L_b)_{Min}}$, the decay paths from $\mathbf{(n,\pi^*)_{Min}}$ to the conical intersections $\mathbf{(^1L_a)_X}$ and $\mathbf{(n,\pi^*)_X}$ have sizable barriers of about 0.1 eV or more. These features of the PES justify the assignment of the experimental short and long lifetimes fluorescence to $\mathbf{(^1L_b)_{Min}}$ and $\mathbf{(n,\pi^*)_{Min}}$, respectively, as shown in Figure 1. The barrier for decay of $\mathbf{(n,\pi^*)_{Min}}$ also explains the dependence of the (n,π*) lifetime (long component of the fluorescence) on the excitation wavelength. The present computations also suggest that the decay of $\mathbf{(n,\pi^*)_{Min}}$ through $\mathbf{(^1L_a)_X}$ is energetically more favorable than the one through $\mathbf{(n,\pi^*)_X}$. Moreover, it appears that a further possibility for $\mathbf{(n,\pi^*)_{Min}}$ is intersystem crossing to the triplet state. This would support the assignment of the triplet state to a species with nanosecond lifetime observed in time-resolved spectroscopy.[5,6]

Computational Details

The calculations follow the CAS-PT2//CASSCF methodology, where the reaction paths (MEPs) are calculated at the CASSCF/ 6-31G* level with Gaussian03[25] and the energetics recalculated at the CAS-PT2 level with MOLCAS-5.4.[26] No symmetry restrictions were applied during the calculations. For the paths discussed in this paper, the "full" active space comprises 16 electrons in 12 orbitals (the 10 π orbitals and the two in-plane lone pairs of the N_1 and N_3 atoms), noted as (16,12). To reduce the computational effort and avoid convergence problems, the CASSCF optimizations and reaction path calculations were carried out with reduced active spaces, keeping only orbitals with occupations between 1.99 and 0.01. Thus, the conical intersections $\mathbf{(^1L_a)_X}$ and $\mathbf{(n,\pi^*)_X}$ were optimized with active spaces of nine orbitals. All optimizations (including intrinsic reaction coordinate calculations) were carried out state averaging over two states with equal weights except for the ground-state optimization (Franck−Condon geometry, FC) and $\mathbf{(^1L_b)_{Min}}$, which were optimized without state averaging, and $\mathbf{(^1L_b/n,\pi^*)_{TS}}$, which was optimized state averaging over three states with equal weights and using the S_1 gradients. Orbital rotation corrections to the gradients were not included in the optimizations with state-averaged orbitals using nine or more orbitals because they require the solution of the coupled perturbed MCSCF equations, which is computationally not feasible for an active space of more than eight electrons with the present Gaussian code. However the contribution of these terms to the gradients should be negligible. Note also that all transition structure optimizations done with active spaces of seven or eight orbitals (see below) do include the orbital rotation terms. The active spaces used in the calculations are summarized in Table SI1 (Supporting Information).

All transition structures were characterized with analytical frequency calculations, which are only feasible with up to eight orbitals with the present Gaussian code. Thus, the optimizations of $\mathbf{(^1L_b/n,\pi^*)_{TS}}$ and $\mathbf{(^1L_b/^1L_a)_{TS}}$ and the corresponding MEP calculations were carried out with active spaces of seven and eight orbitals, respectively. These active spaces lead to satisfying estimations of the CAS-PT2//CASSCF barrier, as discussed below in the Results section. In contrast to this, structures $\mathbf{(n,\pi^*/^1L_a)_{TS}}$ and $\mathbf{(n,\pi^*)_{TS}}$ were calculated with active spaces of ten orbitals, and the corresponding frequencies were calculated with a reduced active space of seven orbitals, after re-optimizing the transition structures with these active spaces.

MEP calculations were started from the transition structures following the analytical force constants in the forward and reverse

(25) Frisch, M. J., et al. *Gaussian03*, revision B.02; Gaussian, Inc.: Pittsburgh, PA, 2003.
(26) Andersson, K., et al. *MOLCAS*, Version 5.4; University of Lund: Sweden, 2003.

Table 1. Vertical and 0−0 Excitation Energies (E), Oscillator Strengths (f), and State Characterization at FC Geometry

	calcd			exptl[a]		
state	E_{vert}[b] [eV]	f	E_{0-0} [eV]	E_{max} [eV]	E_{0-0} [eV]	configurations
(n,π^*)	5.01 (5.92)	0.006	4.35		4.40	$n^- \rightarrow \pi_L$
^1L_b	5.05 (5.42)	0.002	4.71		4.48	$\pi_H \rightarrow \pi_{L+1}$
						$\pi_{H+1} \rightarrow \pi_L$
^1L_a	5.16 (6.94)	0.21		4.92		$\pi_H \rightarrow \pi_L$
(n,π^*)	5.72 (6.44)	0.005				$n^- \rightarrow \pi_{L+1}$

[a] References, see text. [b] CAS-PT2 values, CASSCF in brackets.

Table 2. Relative CAS−PT2 Energies (E_{rel}) of Critical Points, with Respect to Ground-State FC Energy

structure	E_{rel} [eV]
$(^1L_b)_{Min}$	4.71
$(n,\pi^*)_{Min}$	4.35
$(^1L_a)_X$	3.72/4.25[a]
$(^1L_a)_{X,PT2}$	3.92/4.06[b]
$(n,\pi^*)_X$	3.84/4.56[a]
$(n,\pi^*)_{X,PT2}$	4.45/4.55[b]
$(^1L_b/n,\pi^*)_{TS}$	4.67[c]
$(^1L_b/^1L_a)_{TS}$	4.46[d]
$(n,\pi^*/^1L_a)_{TS}$	4.52
$(n,\pi^*)_{TS}$	4.95

[a] S_1 and S_0 energies at CASSCF-optimized point. [b] S_1 and S_0 energies at point near CAS-PT2 degeneracy, see Computational Details. [c] Energy at CASSCF-optimized transition structure, highest energy point along the path: 4.71 eV. [d] Energy at CASSCF-optimized transition structure, highest energy point along the path: 4.72 eV.

directions, using the intrinsic reaction coordinate algorithm implemented in Gaussian.[27,28] In the cases of $\mathbf{(n,\pi^*/^1L_a)_{TS}}$ and $\mathbf{(n,\pi^*)_{TS}}$, which were optimized with large active spaces, the force constants from the analytical frequency calculations with smaller active spaces were used for the MEP. Besides, the MEP for the initial relaxation of the ^1L_b and ^1L_a states from the FC geometry, and for the relaxation paths from the $\mathbf{(^1L_a/^1L_b)_X}$ and $\mathbf{(^1L_a)_X}$ conical intersections, were run with the same algorithm, using the gradients of the relevant states as the initial relaxation direction in the IRC calculation. The MEP for relaxation of the ^1L_a state from the FC geometry to $\mathbf{(^1L_a/^1L_b)_X}$ was calculated with an active space of 10 π orbitals, leaving out the nitrogen n orbitals, as these are doubly occupied for the two (π,π^*) states at planar and quasiplanar geometries. This implies that the (n,π^*) states are effectively neglected in the calculation, but they are included in the CASSCF reference wave function for the CAS-PT2 calculation (see Figure 7 below). Note that exploratory calculations with a larger active space showed that the inclusion of the n orbitals in the active space during the IRC calculation does not change the resulting CAS-PT2//CASSCF profiles significantly, while it makes the computation more tedious because additional crossings between the ^1L_a and the (n,π^*) states appear.

For a reliable estimation of the overall energetics, the CAS-PT2 energies of all structures (critical points and points along the MEP) were calculated with the (16,12) active space, averaging over six states with equal weights in the CASSCF reference calculation, and using a 6-31G* basis. The number of states was chosen in order to include always at least two (π,π^*) and two (n,π^*) excited states in the reference wave function and thereby avoid orbital rotations that would change the composition of the active space. An imaginary level shift parameter of 0.15 was used in all CAS-PT2 calculations. The relative energies of the critical points relative to the ground-state energy at the FC geometry are listed in Table 2, and the corresponding structures are given in the Supporting Information. For the triplet state calculation at $\mathbf{(n,\pi^*)_{Min}}$, a reference function of five states with equal weights was used for the CAS-PT2 calculation, whereas the spin−orbit coupling (SOC) constant was calculated for a CASSCF(16,12) wave function over four states (two singlets and two triplets).

At the conical intersections $\mathbf{(^1L_a)_X}$ and $\mathbf{(n,\pi^*)_X}$, optimized at the CASSCF level, there is an energy gap at the CAS-PT2 level because of the differential correlation between the crossing states. The energy gaps are approximately 0.5 and 0.7 eV, respectively (see Table 2). However the presence of the two seams of intersection could be confirmed at the CAS-PT2 level by locating points with smaller energy gaps near the CASSCF-optimized intersections. The idea is *not* to locate the minimum energy structure of the seams but rather to confirm that the seams exist at the CAS-PT2 level. Thus, a structure on the $\mathbf{(^1L_a)_X}$ seam with a CAS-PT2 energy gap of 0.14 eV was found calculating the S_1 and S_0 gradients at the CASSCF-optimized point and displacing the structure along the gradient difference coordinate. A point with a CAS-PT2 energy gap of 0.10 eV on the $\mathbf{(n,\pi^*)_X}$ seam was located with a similar method. The structures are listed as $\mathbf{(^1L_a)_{X,PT2}}$ and $\mathbf{(n,\pi^*)_{X,PT2}}$ in Table 2 and their coordinates given in the Supporting Information.

Results

Vertical Excitations. The vertical excitations, calculated at the CASSCF optimized FC geometry of C_1 symmetry, are shown in Table 1. Rydberg states have not been considered in the present calculation of vertical excitations. The lowest calculated excited states are two (π,π^*) states and one (n,π^*) state. The (π,π^*) states are usually classified as ^1L_b and ^1L_a, whereas for the $(n,\pi)^*$ state the excitation comes from an orbital which is the antibonding linear combination of the in-plane orbitals of N_1 and N_3 (see Figure 2b). At the CAS-PT2 level, with a CASSCF(16,12) reference function and the 6-31G* basis, the (n,π^*) state is the lowest-lying state. The ^1L_b (π,π^*) state is slightly higher by less than 0.1 eV, and the ^1L_a (π,π^*) state of high oscillator strength lies approximately 0.1 eV higher than the ^1L_b one. The comparison with experiment is satisfactory, as the vertical energy of the ^1L_a state (5.16 eV) is less than 0.3 eV higher than the experimental value (absorption maximum at 252 nm, ie 4.92 eV).[29] Previous calculations of the vertical excitations have been revised in a recent publication.[11] In the present work, the relative order of the vertical (π,π^*) excitations and the small energy difference between them is in agreement with previous calculations obtained with the CAS-PT2,[10,12,30,31] TD-DFT,[32] and DFT/MRCI methods,[11] which give energy gaps of up to approximately 0.3 eV. The relative energy of the lowest-lying (n,π^*) state is similar to previous multireference perturbation configuration interaction (CIPSI),[23] TD-DFT,[32,33] and DFT/MRCI[11] calculations, where it lies within a range of 0.1 eV with respect to the ^1L_b excitation. The CAS-PT2 results from previous publications[10,30,31] give an (n,π^*) excitation which is substantially higher (more than 0.5 eV relative to the ^1L_b state), but this is presumably due to the small size of the CASSCF reference function (10 and 11 orbitals). Here two in-plane orbitals (N_1 and N_3 nitrogen lone pairs, see Computational Details) have been included in the reference wave function for a better description of the (n,π^*) state, and the most recent CAS-PT2 (n,π^*) vertical excitation from the literature,[12] calculated with a similar reference active space, is close to the present value (0.2 eV over the ^1L_b state). Moreover, the vertical CAS-PT2 excitations of the ^1L_b and (n,π^*) states, calculated with

(27) González, C.; Schlegel, H. B. *J. Chem. Phys.* **1989**, *90*, 2154−2161.
(28) González, C.; Schlegel, H. B. *J. Phys. Chem.* **1990**, *94*, 5523−5527.
(29) Clark, L. B.; Peschel, G. G.; Tinoco, I. *J. Phys. Chem.* **1965**, *69*, 3615.
(30) Broo, A.; Holmen, A. *J. Phys. Chem. A* **1997**, *101*, 3589−3600.
(31) Fülscher, M. P.; Serrano-Andrés, L.; Roos, B. O. *J. Am. Chem. Soc.* **1997**, *119*, 6168−6176.
(32) Sobolewski, A. L.; Domcke, W. *Eur. Phys. J. D* **2002**, *20*, 369−374.
(33) Shukla, M. K.; Leszczynski, J. *J. Comput. Chem.* **2004**, *25*, 768−778.

the 6-311+G** basis, vary by less than 0.1 eV, which shows that the effect of enlarging the basis set is small. Overall, this supports the conclusion that the reference space of 12 orbitals used here gives a balanced treatment of the relevant excited states.

Critical Points on the S_1 Surface and Characterization of the States. Two local minima were optimized at the CASSCF level on the S_1 surface, one for the ^1L_b and one for the (n,π^*) state, labeled as $\mathbf{(^1L_b)_{Min}}$ and $\mathbf{(n,\pi^*)_{Min}}$, respectively. $\mathbf{(^1L_b)_{Min}}$ has a quasiplanar structure, while for $\mathbf{(n,\pi^*)_{Min}}$, C_2 is bent out of plane and pyramidalized (see Figure 1), as described previously.[10−12] The orbitals involved in the excitations at the geometry of the two respective minima are displayed in parts a and b of Figure 2, respectively. The ^1L_b wave function is dominated by configurations with excitations from a_1 to a_3 and a_2 to a_4 (see Figure 2a for the labeling), which corresponds, approximately, to the highest occupied molecular orbital (HOMO)-1 to lowest-unoccupied molecular orbital (LUMO) and HOMO to LUMO+1 excitations in terms of the ground-state molecular orbitals. The calculated 0−0 excitation energies for the two states are shown in Table 1 and compared with the experimental values. Experimentally, the lowest vibronic transition is assigned to the (n,π^*) state, and the value is 4.40 eV (approximately 35 500 cm^{-1}),[13,16,17] which agrees well with the calculated energy of 4.35 eV. For the 0−0 vibronic transition of the (π,π^*) state, the agreement is not as good. The calculations give a value of 4.71 eV, which is higher than the value assigned experimentally at 4.48 eV.

To estimate the possibility of populating the triplet state from the longer-living intermediate $\mathbf{(n,\pi^*)_{Min}}$, the energies of the lowest triplets and the SOC with the (n,π^*) state were calculated at the CAS-PT2 and CASSCF levels, respectively (see Computational Details). At the CAS-PT2 level, the two lowest triplet states are degenerate to within less than 0.01 eV and lie approximately 0.04 eV lower than S_1 at the geometry of $\mathbf{(n,\pi^*)_{Min}}$. One of the triplets is of predominant (π,π^*) character, while the other one is predominantly (n,π^*). As one can predict from El-Sayed's rules,[34] there is a larger SOC of S_1 with the ^{3}(π,π^*) state (approximately 13 cm^{-1}), than with the ^{3}(n,π^*) state (approximately 4 cm^{-1}). Overall the region of $\mathbf{(n,\pi^*)_{Min}}$ may provide access to the ^{3}(π,π^*) state, since the calculations suggest the presence of a near intersystem crossing point with substantial SOC between the ^{1}(n,π^*) and ^{3}(π,π^*)states.

In addition to the minima, two conical intersections with the ground state were optimized that correlate, approximately, with the ^1L_a and (n,π^*) states, labeled as $\mathbf{(^1L_a)_X}$ and $\mathbf{(n,\pi^*)_X}$, respectively. The two structures are heavily bent out of plane, as already described:[10−12] $\mathbf{(^1L_a)_X}$ is characterized by the bending of C_2, while for $\mathbf{(n,\pi^*)_X}$ the N_1 atom and the amino substituent on C_6 are bent out of plane in opposite directions. The orbitals involved in the excitations at the two structures are shown in parts c and d of Figure 2, respectively. For $\mathbf{(^1L_a)_X}$, the orbitals involved in the excitation correlate, approximately, with the HOMO and LUMO of the molecule in the FC region (a_2 and a_3 in Figure 2a). There is also some mixing with the in plane n orbitals due to the out-of-plane bending of C_2. The correlation of $\mathbf{(^1L_a)_X}$ with the corresponding state at the FC geometry is confirmed by the MEP calculation from the FC geometry to the intersection (see below). The characterization of $\mathbf{(n,\pi^*)_X}$ is based on the n character of the orbital involved in the excitation (Figure 2d). The orbital in question, which has a mixed π/n character due to the out-of-plane bend of N_1, is localized on this atom. This suggests that $\mathbf{(n,\pi^*)_X}$ corresponds to a different electronic state than $\mathbf{(n,\pi^*)_{Min}}$, which probably explains the presence of a barrier between both structures. Mechanistically, this conical intersection is of the same type as one found for cytosine, which involves an (n,π^*) excitation from a nitrogen adjacent to a carbon bearing an amino substituent.[35] As in cytosine, the out-of-plane bending of N_1 and the amino group can be understood as an effect of the electronic repulsion between the N_1 and C_6 π orbitals, caused by the excitation.

MEPs and Energy Barriers on S_1. With the purpose of estimating the energy barriers associated to the different decay paths, the transition structures were optimized on the S_1 surface for the four relevant paths, at the CASSCF level, and the associated MEPs were calculated. Methods for scanning the PES other than MEP, based on linear interpolations or relaxed scans along constrained coordinates, can lead to misleading conclusions in multidimensional reaction coordinates such as the ones studied here, whereas the MEP calculations provide a rigorous description of the reaction paths. The recalculation of the CAS-PT2 energies along the CASSCF minimum energy path can be problematic, especially when the state order changes between the two levels of theory. However this is not the case for the paths on S_1 calculated here. Therefore the results discussed below should provide a reliable overview of the energetics of the S_1 surface. Moreover, the present results show that the paths can be described as adiabatic processes on the S_1 PES. They involve "switches" between different states, but in all cases transition structures (TS) between the different critical points (minima or conical intersections) exist. For these adiabatic processes, the present description in terms of TS and MEP is better than a description based on conical intersections between the "switching" states (of the S_2/S_1 type here) because at the TS the energy gaps are considerable (more than approximately 0.4 eV in the cases discussed here) and transitions to the upper state are unlikely.

Two of the optimized TSs connect $\mathbf{(^1L_b)_{Min}}$ with $\mathbf{(n,\pi^*)_{Min}}$ and the conical intersection $\mathbf{(^1L_a)_X}$. They are labeled $\mathbf{(^1L_b/n,\pi^*)_{TS}}$ and $\mathbf{(^1L_b/^1L_a)_{TS}}$, respectively. The two other TS separate $\mathbf{(n,\pi^*)_{Min}}$ from the $\mathbf{(^1L_a)_X}$ and $\mathbf{(n,\pi^*)_X}$ conical intersections and are labeled $\mathbf{(n,\pi^*/^1L_a)_{TS}}$ and $\mathbf{(n,\pi^*)_{TS}}$. A TS between $\mathbf{(^1L_b)_{Min}}$ and $\mathbf{(n,\pi^*)_X}$ could not be located in the present study. All TS were characterized with analytical frequency calculations (see Computational Details), and the MEP for the four reaction paths were calculated with the intrinsic reaction coordinate method. The resulting CAS-PT2//CASSCF energy profiles (energy in eV relative to the ground-state energy at the FC geometry, against displacements in atomic units) are shown in Figures 3−6, while the CASSCF energy profiles of the CASSCF(16,12) reference function (see Computional Details) are shown in the Supporting Information (Figures SI1−SI4). The reaction coordinates are composed of changes in the bond lengths and the angles (mainly torsions) of the molecule. For a better understanding of the changes involved, the reader is referred to Figure 1, where the structures connected by the different paths are displayed. Because of differential correlation (see Computational Details), the paths in the direction of

(34) Lower, S. K.; Elsayed, M. A. *Chem. Rev.* **1966**, *66*, 199.
(35) Ismail, N.; Blancafort, L.; Olivucci, M.; Kohler, B.; Robb, M. A. *J. Am. Chem. Soc.* **2002**, *124*, 6818−6819.

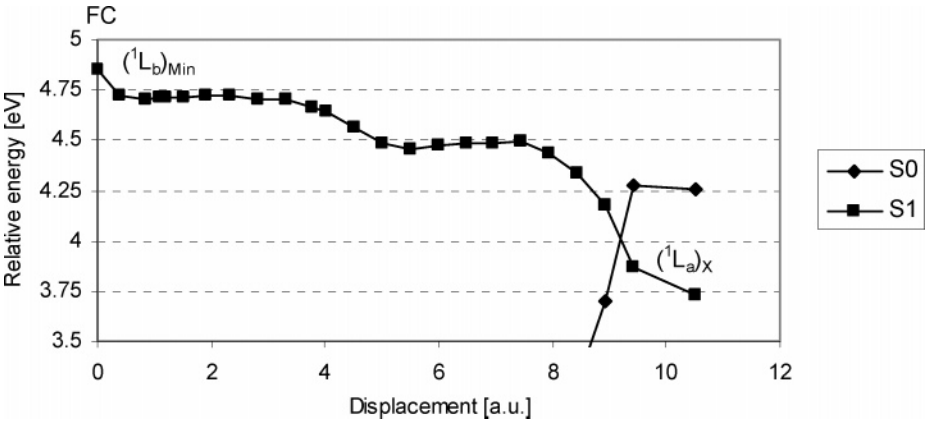

Figure 3. CAS-PT2//CASSCF energy profile along the MEP for decay of the ^1L_b state from the FC geometry to $(^1L_a)_X$ through $(^1L_b)_{Min}$.

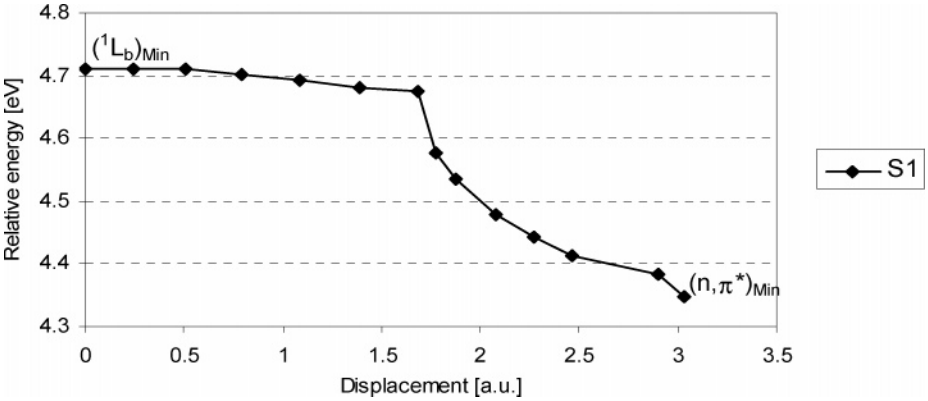

Figure 4. CAS-PT2//CASSCF energy profile along the MEP from $(^1L_b)_{Min}$ to $(n,\pi^*)_{Min}$.

the conical intersections do not end at points of CAS-PT2 degeneracy, but the existence of the corresponding seams at the CAS-PT2 level has been proved in separate calculations (see Computational Details).

Figures 3 and 4 show the two paths from $(^1L_b)_{Min}$ to $(^1L_a)_X$ and $(n,\pi^*)_{Min}$, respectively. The corresponding transition structures have not been reported previously. Figure 3 also includes the path from the FC structure to $(^1L_b)_{Min}$. At the CAS-PT2//CASSCF level, the two paths are virtually barrierless (0.02 eV or less), although at the CASSCF level there are barriers of 0.10 and 0.21 eV, respectively. The shape of the CAS-PT2 energy profiles indicates that the actual paths at that level may have a different curvature in the multidimensional coordinate space. This may be also related to the use of smaller active spaces (seven and eight orbitals) in these MEP calculations (see Computational Details). Besides, the fact that $(^1L_b)_{Min}$ was not optimized at the CAS-PT2 level implies that there might be small barriers for the paths at the CAS-PT2 level. However the main point is to show that there are substantial differences between the barriers for the decay paths from $(^1L_b)_{Min}$ and the ones from $(n,\pi^*)_{Min}$ (see below), and this should not be affected by the approximations just mentioned.

The CAS-PT2//CASSCF energy profiles for the paths from $(n,\pi^*)_{Min}$ to $(^1L_a)_X$ and $(n,\pi^*)_X$ are shown in Figures 5 and 6, respectively. These paths have barriers of 0.17 and 0.60 eV. The shape of the CAS-PT2 energy profiles is similar to the CASSCF ones (see Figures SI3 and SI4, Supporting Information). In one of the previous CAS-PT2//CASSCF studies, the barrier between $(n,\pi^*)_{Min}$ and $(^1L_a)_X$, based on single-point calculations on the optimized minimum and transition structure,

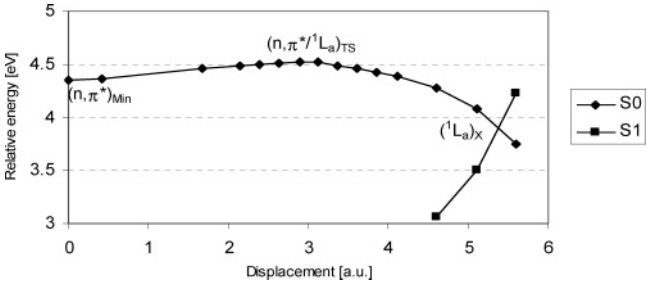

Figure 5. CAS-PT2//CASSCF energy profile along the MEP from $(n,\pi^*)_{Min}$ to $(^1L_a)_X$.

disappears at the CAS-PT2 level.[10] A possible reason for the discrepancy with the present results could be differences in the optimization methods which result in different structures. Calculations at the present CAS-PT2 level with the structures reported in that study[10] for the (n,π*) minimum and the TS show that the energy of the (n,π*) minimum could be somewhat overestimated there, whereas the energy of the TS could be overestimated here by approximately 0.1 eV. On the other hand, the other preceding CAS-PT2//CASSCF study gives a barrier of 0.14 eV.[12] Overall one can conclude that approximately 0.1 eV are a good estimate for the barrier between $(n,\pi^*)_{Min}$ and $(^1L_a)_X$. Note that the ring planar structure reported[10] as the equivalent of the one labeled $(n,\pi^*)_{TS}$ here is actually the TS between two mirror images of the $(n,\pi^*)_X$ intersection.

Decay of the ^1L_a State. The ^1L_a state is the spectroscopically active state. The MEP from the FC structure, calculated at the CASSCF, is barrierless and ends at a conical intersection with the ground state, $(^1L_a)_X$. The CASSCF calculations are shown

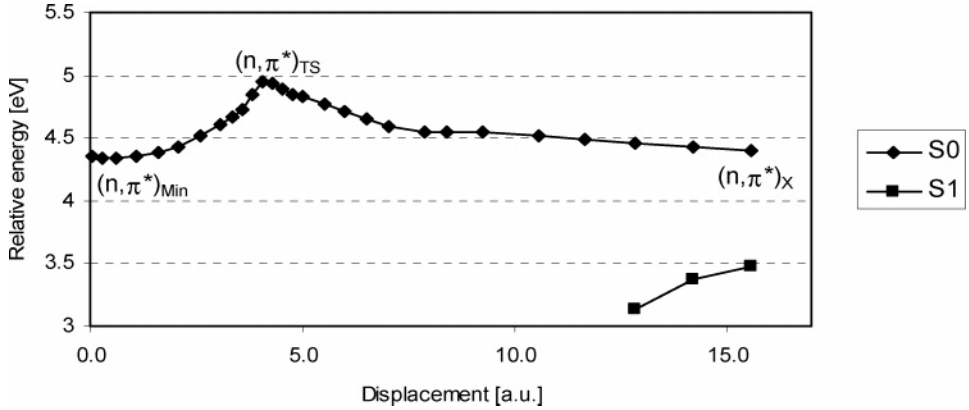

Figure 6. CAS-PT2//CASSCF energy profile along the MEP from $\mathbf{(n,\pi^*)_{Min}}$ to $\mathbf{(n,\pi^*)_X}$.

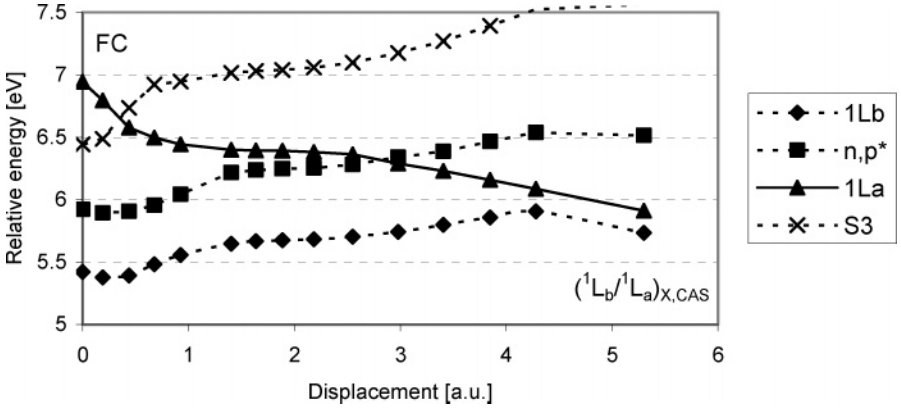

Figure 7. CASSCF energy profile along the MEP on the ^1L_a from the FC geometry to $\mathbf{(^1L_b/^1L_a)_X}$.

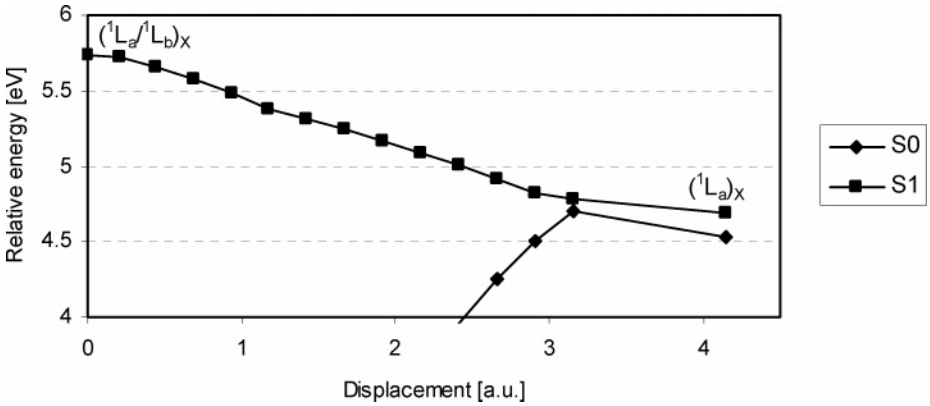

Figure 8. CASSCF energy profile along the MEP from $\mathbf{(^1L_b/^1L_a)_X}$ to $\mathbf{(^1L_a)_X}$.

in Figures 7 and 8. The first part of the MEP leads to a conical intersection between the two states, $\mathbf{(^1L_a/^1L_b)_X}$. From this point, a MEP on the S_1 surface following the gradient of the ^1L_a state leads to the crossing with the ground state, $\mathbf{(^1L_a)_X}$. This MEP has no barrier. Thus at the CASSCF level there is a barrierless decay path from the FC geometry to $\mathbf{(^1L_a)_X}$ that goes through the conical intersection $\mathbf{(^1L_a/^1L_b)_X}$. However this crossing has a peaked shape,[36] and there is a further MEP that leads from there to $\mathbf{(^1L_b)_{Min}}$ (Figure SI5, Supporting Information). Branching between the two alternative routes (decay to $\mathbf{(^1L_a)_X}$ or $\mathbf{(^1L_b)_{Min}}$) is possible at $\mathbf{(^1L_a/^1L_b)_X}$ because the (orthogonalized) gradient difference and interstate coupling vectors, the two vectors that give rise to the conical shape of the intersection,[37] have similar lengths (0.15 and 0.09 atomic units at the CASSCF level, respectively). Thus, in a semiclassical picture, trajectories that go through the intersection have a finite possibility of branching along the slope of the ^1L_b state and populate the region of $\mathbf{(^1L_b)_{Min}}$. In principle the same is possible at the intersection $\mathbf{(^1L_a/n,\pi^*)_X}$, which occurs earlier along the profile of Figure 7, but this has not been considered here in detail.

To confirm the existence of the barrierless decay path for the ^1L_a state at the CAS-PT2//CASSCF level, single-point calculations have been carried out along the MEP from the FC geometry to $\mathbf{(^1L_a/^1L_b)_X}$ (Figure 9). The energy profile for the ^1L_a state of interest does not reproduce the CASSCF one but shows a discontinuous behavior and an energy rise. This is an effect of the proximity of the states and the different positions of the ($^1L_a/^1L_b$) intersections at the CASSCF and CAS-PT2 level. However the ^1L_a and ^1L_b states do cross early along the CAS-PT2//CASSCF energy profile of the MEP (see Figure 9), at

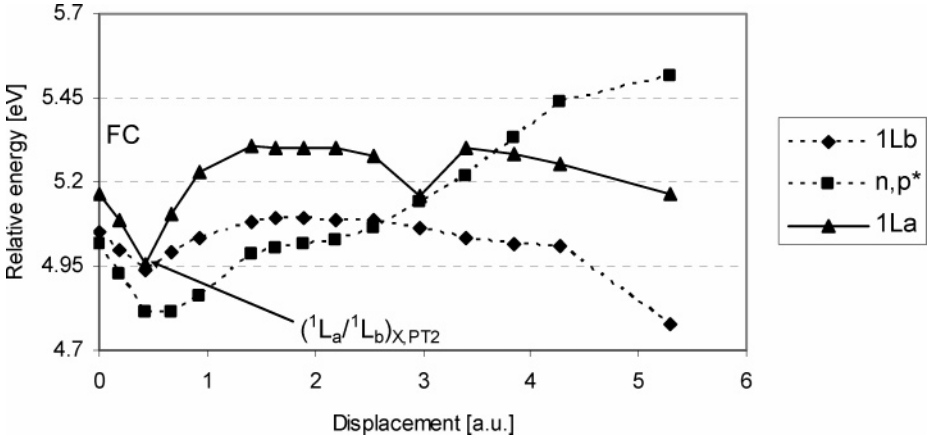

Figure 9. CAS-PT2//CASSCF energy profile along the MEP on the ^1L_a state from the FC geometry to $(^1L_b/^1L_a)_X$.

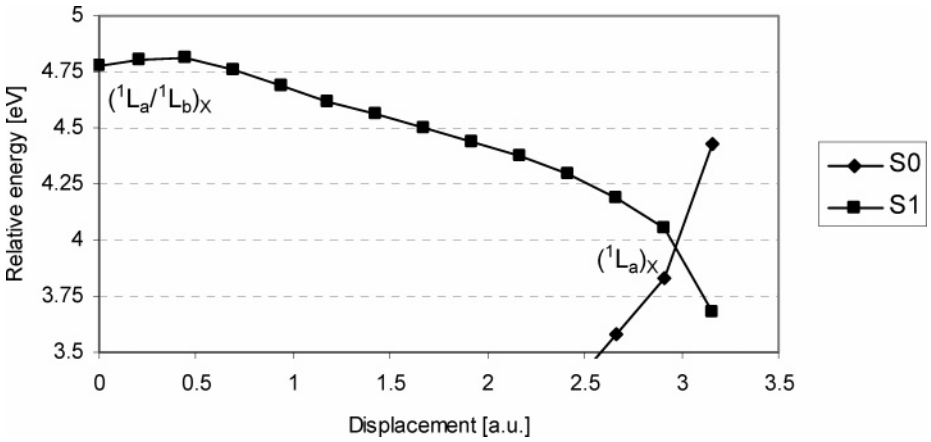

Figure 10. CAS-PT2//CASSCF energy profile along the MEP from $(^1L_b/^1L_a)_X$ to $(^1L_a)_X$.

energies lower than the ^1L_a vertical excitation. Moreover, the CAS-PT2 energy profile along the MEP from $(^1L_a/^1L_b)_X$ to $(^1L_a)_X$ (Figure 10) shows an almost continuous decrease, apart from an initial energy rise of less than 0.05 eV. Overall, this is a fair indication that the barrierless decay path of the ^1L_a state to the ground state is a "real" feature of the PES and not an artifact of the CASSCF level of theory, although more solid proof can only be provided by calculations at a higher level.

Decay from $(^1L_a)_X$ on the Ground State. The possibility of photodegradation after decay at a conical intersection can be estimated by determining the ground-state MEP from the intersection. $(^1L_a)_X$ has an intermediate topology, using the classification of Ruedenberg and co-workers.[36] Thus, the intersection coincides, approximately, with a minimum on the excited state, and there is only one decay path on the ground state. This was confirmed by exploring the branching space of the intersection, which determines the initial directions of the decay. A series of calculations was run, at the CASSCF level, at single points lying in the plane formed by the gradient difference and interstate coupling vectors. These points form a circle around the intersection, and only one ground-state decay channel appears along the circle (see Figure SI6, Supporting Information). An IRC calculation along this channel leads to the FC geometry (see Figure SI7, Supporting Information). No direct paths to other products could be located. This suggests that the formation of photochemical products during the decay at $(^1L_a)_X$ is unlikely, although reactions of the hot molecules formed in the decay cannot be excluded.

Discussion

The present computational study focuses on the surface topography of the first excited state of adenine, i.e., the critical points, the minimum energy paths that connect them, and the associated energy barriers. In the CAS-PT2//CASSCF methodology used here, dynamic correlation, which is essential for a good estimate of the energies, is included a posteriori by single-point calculations on the CASSCF structures. This approximation has its shortcomings when the CASSCF paths differ significantly from the CAS-PT2 ones, which is the case for some of the reaction paths presented here. However, the main goal of providing a good estimate and distinguishing between the energetics along the different reaction paths has been accomplished, as discussed in the previous section. Thus the accuracy of the CAS-PT2 method is approximately 0.1−0.2 eV, which is the amount by which the different barriers differ. Therefore the present computational results should provide a sufficiently solid basis for a discussion of the experimental results.

The CASSCF calculations for the ^1L_a state, which has the highest oscillator strength, suggest that upon absorption this state will decay straight to the ground state through $(^1L_a)_X$, as previously proposed.[10] Although this needs confirmation at a higher level of theory, it would imply that the ^1L_a state would

(36) Atchity, G. J.; Xantheas, S. S.; Ruedenberg, K. *J. Chem. Phys.* **1991**, *95*, 1862−1876.
(37) Bernardi, F.; Olivucci, M.; Robb, M. A. *Chem. Soc. Rev.* **1996**, *25*, 321-&.

only have a small "direct" contribution to the decay signal. However it could contribute "indirectly" to the fluorescence or ionization signal. Thus excitation of the ^1L_a state may induce population of the ^1L_b state (and possibly the (n,π^*) one) when passing through the corresponding conical intersections, as discussed in the Results section.

Experimentally, the ultrafast part of the decay is fitted to a double exponential with two lifetimes, where the short component (approximately 0.1 ps) corresponds to $\mathbf{(^1L_b)_{Min}}$ and the longer one (1−2 ps) to $\mathbf{(n,\pi^*)_{Min}}$.[5−9] This corresponds to the stepwise formation of the $\mathbf{(n,\pi^*)_{Min}}$ intermediate from the $\mathbf{(^1L_b)_{Min}}$ one,[8] which is in agreement with the present and previous computations. The calculations show that the decay through $\mathbf{(^1L_a)_X}$ will be the preferred decay route for $\mathbf{(n,\pi^*)_{Min}}$, since the alternative decay through $\mathbf{(n,\pi^*)_X}$ is substantially higher. The barrier calculated here for the decay of $\mathbf{(n,\pi^*)_{Min}}$ also explains the decrease of the longer component lifetime when the excitation energy is increased (from 272 to 267 nm).[8]

The existence of two competing channels for the $\mathbf{(^1L_b)_{Min}}$ decay can explain the observed wavelength dependence of the relative amplitude of the ^1L_b component in the decay. Its amplitude with respect to the (n,π^*) one decreases significantly at higher excitation energies (from 267 to 250 nm).[6] This has been interpreted in terms of an additional decay channel for $\mathbf{(^1L_b)_{Min}}$ that involves dissociation of the N_9−H bond, driven by a low-lying (π,σ^*) state.[6,8,21,38,39] This channel would become significant at higher excitation energies. The energetics for this path have been not considered here because the 6-31G* basis used here is not adequate to describe it, but recent CAS-PT2[24] and DFT/MRCI[11] calculations have established that the energy threshold for the dissociation lies around 5.4 eV (approximately 230 nm). Thus, NH dissociation via tunneling has been proposed to account for the decrease of the ^1L_b amplitude at 250 nm. In fact hydrogen atoms generated by the NH dissociation have been detected experimentally after excitation at lower energies (267 and 241 nm).[38,40] However the time scale for the measured hydrogen loss is of the order of nanoseconds[40] compared to the excited state lifetime of approximately 1 ps, which could imply that it is not an excited-state process but a reaction of the hot molecules produced in the radiationless decay.

In any case, the occurrence of NH dissociation via tunneling cannot be excluded on the basis of the present calculations. However an alternative explanation for the wavelength dependence of the ^1L_b amplitude that is not based on the NH channel can be offered. Thus the postulated additional channel could well be the decay of $\mathbf{(^1L_b)_{Min}}$ through $\mathbf{(^1L_a)_X}$, and the wavelength dependence of the ^1L_b amplitude could reflect differences in the branching between the $\mathbf{(n,\pi^*)_{Min}}$ and $\mathbf{(^1L_a)_X}$ channels of $\mathbf{(^1L_b)_{Min}}$ depending on the excitation wavelength. In turn this will cause different ratios in the population of the ^1L_b and (n,π^*) species, explaining the different relative amplitudes. Although such a proposal can only be confirmed by dynamics calculations, it appears as a reasonable alternative to the explanation based on the NH dissociation channel.

In a turn to discussion of solvent effects, the 9H tautomer of adenine in water solution has a monoexponential lifetime of 180 fs.[20] The disappearance of the picosecond (n,π^*) component in water can be explained with the energy raise of that state induced by the solvent. This may induce a barrier for the decay of $\mathbf{(^1L_b)_{Min}}$ to $\mathbf{(n,\pi^*)_{Min}}$, blocking that channel and leaving the direct decay of $\mathbf{(^1L_b)_{Min}}$ through $\mathbf{(^1L_a)_X}$ as the only significant channel.

The calculations also suggest that the triplet state can be populated from $\mathbf{(n,\pi^*)_{Min}}$, which may explain the experimental observation of a nanosecond component. This component has been observed in the time-resolved photoelectron spectrum of adenine,[6] although the addition of this component to the spectral fit has been put into question in a different study.[7] A triplet state has been suggested as the detected species. The computations show that at $\mathbf{(n,\pi^*)_{Min}}$ there are two close-lying triplets with an energy gap of less than 0.1 eV with respect to the singlet state. One of the states is of (π,π^*) character, and the SOC is approximately 13 cm^{-1}. This suggests that in the vicinity of $\mathbf{(n,\pi^*)_{Min}}$ the intersystem crossing to the $^3(\pi,\pi^*)$ state is possible, thus explaining the appearance of the nanosecond component. The details of the intersystem crossing and the fate of the triplet (decay to the ground state or photochemical processes) will be the subject of a future study. Moreover, intersystem crossing yields of about 0.1% have been measured for the triplet state formation in water.[41] It is not clear if the present mechanism, which explains the formation of the triplet state through the singlet (n,π^*) state, is also valid in water.

Conclusions

The ongoing development of spectroscopic methods has allowed for a progressively more refined description of the photophysics of 9H adenine in recent years. The computational techniques available for excited-state PES analysis can be used to support this development and help to determine the models to explain the experiments. In the present CAS-PT2//CASSCF study the MEPs on the S_1 surface have been determined together with the associated energy barriers. The results provide computational evidence for the presence of three excited-state decay paths with low barriers for the ^1L_b and (n,π^*) species. Mechanistically, the paths correspond to "switches" between different states, but as a result of vibronic coupling they can be described as adiabatic paths on the S_1 surface through transition structures. This makes the passage from one excited-state structure to the other more efficient because diabatic recrossing between the states is very unlikely, and it shows that vibronic interactions between the excited states are important in the decay.

An exact theoretical description of the excited state dynamics and the complex adenine photophysics can only be provided by dynamics calculations on an accurate surface. However, in a semiclassical picture, the decay rates and the lifetimes of the different intermediates depend on the energy barriers. The present calculations provide a detailed description of the energy surface. Thus they allow to suggest the following rationalization of the experimentally observed decay, which has two components in the picosecond and sub-picosecond range and possibly a third one in the nanosecond range.[5−9,15] The excited-state surface contains a "plateau" that corresponds to a minimum (or quasiminimum) of the ^1L_b state. This region is separated by very low or no barriers from the minimum of the (n,π^*) state

(38) Hünig, I.; Plützer, C.; Seefeld, K. A.; Löwenich, D.; Nispel, M.; Kleinermanns, K. *Chemphyschem* **2004**, *5*, 1427−1431.
(39) Nielsen, S. B.; Solling, T. I. *Chemphyschem* **2005**, *6*, 1276−1281.
(40) Zierhut, M.; Roth, W.; Fischer, I. *Phys. Chem. Chem. Phys.* **2004**, *6*, 5178−5183.
(41) Cadet, J.; Vigny, P. In *Bioorganic Photochemistry*; Morrison, H., Ed.; John Wiley & Sons: New York, 1990; Vol. 1, pp 1−272.

and the conical intersection of ^1L_a character, and the ultrafast component of the excited-state lifetime (approximately 100 fs) originates in the plateau. In contrast to this, for the (n,π*) state there is a proper well, separated by a barrier of 0.1−0.2 eV from the ^1L_a intersection, which gives rise to the component with a lifetime of approximately 1 ps or more. Apart from decay to the ground state, population of a triplet excited state is possible from the (n,π*) state minimum, possibly giving rise to a nanosecond component. The dependence of the lifetime of the (n,π*) component on the excitation energy is clearly due to the barrier calculated for the decay. In addition to that, the wavelength dependence of the relative amplitudes of the two fast components may be explained with the branching between the two alternative routes for decay from the plateau rather than with the NH dissociation driven by a (π,σ*) state.

Acknowledgment. The present research has been supported by the Ramón y Cajal program from the Spanish Ministerio de Educación y Ciencia (MEC) and by Grants BQU2002-04112-C02-02 and BQU2002-03334 from the Dirección General de Investigación (MEC).

Supporting Information Available: Active spaces (Table SI1) and absolute energies of the structures in hartrees (Table SI2), CASSCF energy profiles along the S_1 MEP (Figures SI1−SI4), CASSCF profile for $(^1L_a/^1L_b)_X$ to $(^1L_b)_{Min}$ decay (Figure SI5), and MEP for S_0 decay (Figures SI6 and SI7), Cartesian coordinates of the structures and lowest analytical frequencies for all TS. Complete refs 25 and 26. This material is available free of charge via the Internet at http://pubs.acs.org.

JA054998F